Characterization of EM Downhole-to-Surface Communication Links

F. N. Trofimenkoff, *Senior Member, IEEE*, Michael Segal, Allan Klassen, and J. W. Haslett, *Senior Member, IEEE*

***Abstract*—A downhole-to-surface communication channel consisting of a long vertical cylinder (the stem) and an isolated downhole in-line cylinder (the electrode) embedded in a homogeneous earth is considered in this work. A signal voltage is applied between the electrode and stem, and the received voltage is picked up at the surface between the stem and a ground point or between two ground points. The analysis includes consideration of conductor longitudinal and surface impedance, joint resistance, voltage source resistance, and earth propagation effects to provide a realistic model for assessing the performance of the communication channel for measurement-while-drilling, drill stem testing, and production testing in oil and gas industry applications. Simulation results indicate that consideration of all of these effects is imperative for satisfactory modeling.**

***Index Terms*—Down-hole-to-surface communication, drill stem testing, measurement-while-drilling, production testing.**

I. Introduction

WIRELESS downhole-to-surface communication provides substantial benefits to the oil and gas industry in measurement-while-drilling, drill stem testing, and production testing situations. In this work, a method of dealing with the behavior of a contained vertical cylindrical conductor (a well casing or drill stem) in a homogeneous earth [1]–[4] is used to analyze a communication channel that consists of a voltage source applied between a short section of the lower end of a conducting cylinder (an electrode) and a relatively long upper end (a stem) extending to the surface of the Earth as shown in Fig. 1. The surface receiver senses the potential between the cylinder and a ground point or between two ground points. The voltage source can be coupled into the cylinder directly by providing an insulating break between the stem and electrode or inductively by using the cylinder-earth system as a single turn secondary of a transformer as shown in Fig. 2 [5]. The method described here is very general in that the effects of cylinder longitudinal impedance, cylinder surface impedance, joint resistance, source resistance, and earth propagation effects are included. Results of channel attenuation and driving point impedance calculations for a typical oilfield situation are presented.

II. Problem Definition

The objective of the analysis is to determine the voltage at an arbitrary location on the surface of a homogeneous earth in the presence of an embedded cylindrical vertical conductor with an in-line voltage source as shown in Fig. 1. The stem is taken to have an outer radius "a" and an overall length l_1. The electrode has a length l_e and the same radius as the stem. In carrying out a dc analysis, it is first assumed that the conductor (stem and electrode) have no longitudinal, joint or surface resistance and that the voltage source has no internal resistance. In the next step, longitudinal, surface, joint, and voltage source internal resistance effects are included. Finally, frequency effects are considered by using longitudinal and surface impedance and including earth propagation effects to complete an analysis valid for practical operating conditions.

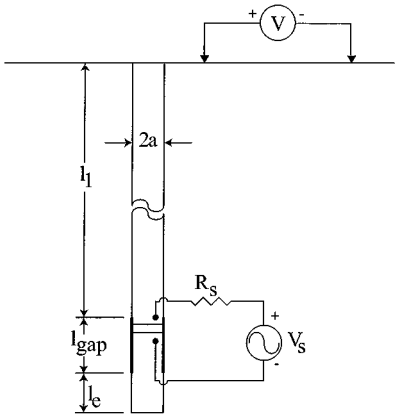

Fig. 1. Embedded vertical conductor with an in-line voltage source.

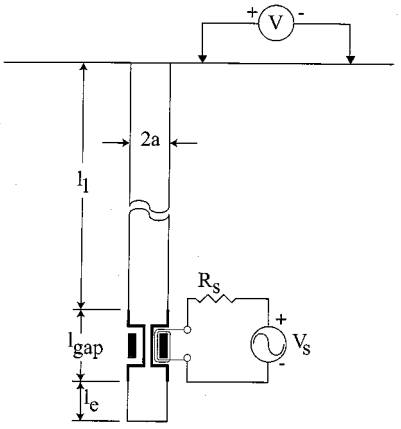

Fig. 2. Inductively generated source voltage.

The half-space problem can be simplified by using the method of images in which a vertical conductor of twice the original length is embedded in a conductive full space and two in-line voltage sources are installed as shown in Fig. 3. The double-length stem is divided into M sections (M odd) of length $2l_1/M$ each, and each electrode is divided into

Manuscript received August 10, 1999; revised March 21, 2000.

The authors are with the Department of Electrical and Computer Engineering, University of Calgary, Calgary, AB T2N 1N4, Canada (trof@enel.ucalgary.ca).

Publisher Item Identifier S 0196-2892(00)07163-1.

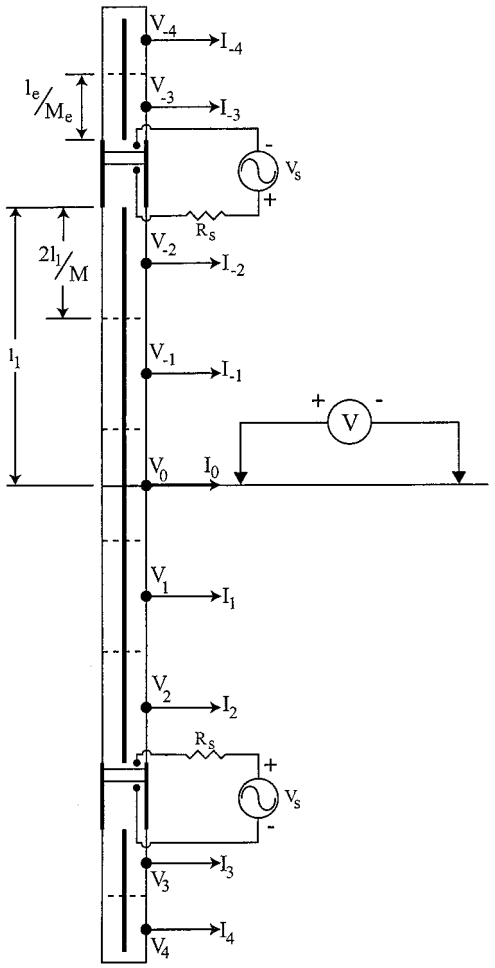

Fig. 3. Division of the stem and electrode into nine elements.

M_e sections. The center point of the outer surface of the nth section will reach a potential V_n where n ranges from 0 to $\pm((M-1)/2+M_e)$. These potentials will have values such that the net current flowing into the physical (half-space) stem and electrode will be zero. The current flow into or out of each section will be a function of the depth of the section, but will, because of symmetry, be uniformly distributed radially. In a manner analogous to substitution theory in electrical circuit analysis, the conductors may be removed and replaced by line current sources. The magnitudes of the line current sources are adjusted so that the potential at the surface of the midpoint of the nth section is V_n.

Once the values of the line current sources are determined, the voltage that appears between the top of the conductor and an arbitrary point on the surface of the homogeneous earth can be determined using the appropriate transfer resistances. Furthermore, the relationship between the voltage source V_s and the current flowing into the electrode can also be established. This information is sufficient to fully characterize the communication channel consisting of the conductor-earth system, the subsurface voltage source, and the surface antenna. Since the analysis that is used relies heavily on line current source modeling, a line current source embedded in a homogeneous earth is now examined.

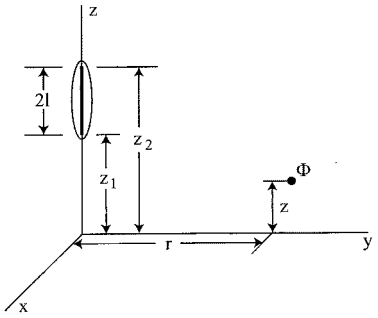

Fig. 4. Uniform line current source of total strength I_s in an infinite earth generating a field point potential. The ellipse represents the source's equipotential surface.

III. Line Current Source Modeling

Consider the situation shown in Fig. 4 where a line current source of total strength I_s is located in an infinite homogeneous earth of resistivity ρ. The potential Φ at a field point (x, y, z) with respect to infinity can be calculated by noting that [6]

$$\Phi = \frac{I_s\rho}{8\pi l}\int_{z_1}^{z_2}\frac{d\lambda}{((\lambda-z)^2+r^2)^{1/2}} \tag{1}$$

$$= \frac{I_s\rho}{8\pi l}\ln\left[\frac{(z_2-z_1)+\sqrt{(z_2-z)^2+r^2}}{(z_1-z)+\sqrt{(z_1-z)^2+r^2}}\right] \tag{2}$$

where $l=((z_2-z_1)/2)$. In the plane $z=0$

$$\Phi = \frac{I_s\rho}{8\pi l}\ln\left[\frac{z_2+\sqrt{{z_2}^2+r^2}}{z_1+\sqrt{{z_1}^2+r^2}}\right]. \tag{3}$$

If the line source is symmetrically disposed about the plane $z=0$, (3) becomes

$$\Phi = \frac{I_s\rho}{4\pi l}\ln\left[\frac{l+\sqrt{l^2+r^2}}{r}\right]. \tag{4}$$

The quantity Φ/I_s is the transfer resistance between a line current source and a field point. The equipotentials are prolate ellipsoids of revolution that can be used to model elemental sections of the stem and electrode, provided the length of the section is large compared to the radius of the cylinder so that the overlaps at the ends of the sections are negligible [6].

IV. Analysis Method

Suppose the cylinder is replaced by nine (chosen for illustrative purposes) line current sources with voltage sources V_s between the double-space stem and each electrode, as shown in Fig. 3. The potential at the surface of the prolate ellipsoid of revolution that models the elemental cylinder will be given by the summation of the contributions to the potential from all of the elemental line current sources. An initial matrix formulation for a perfectly conducting stem and electrode with no metal-earth interface resistance can be written using only the expressions for the self-transfer resistance of elements and the transfer resistances between them. Using (4), the resistance between the

surface of the elemental cylinder and the point at infinity can be written as

$$R_0 = \frac{\rho M}{4\pi l_1} \ln\left(\frac{l_1 + \sqrt{{l_1}^2 + M^2 a^2}}{Ma}\right) \tag{5}$$

where l and r in (4) have been replaced by l_1/M, one half of the elemental section length, and a, the radius of the cylinder. Using (2), the transfer resistance between different stem sections can be written as

$$R_p = \frac{\rho M}{8\pi l_1} \ln\left[\frac{2p+1+\sqrt{(2p+1)^2+\left(\frac{Ma}{l_1}\right)^2}}{2p-1+\sqrt{(2p-1)^2+\left(\frac{Ma}{l_1}\right)^2}}\right] \tag{6}$$

where $p = 1$ to $M-1$. For the self-transfer resistance of an electrode element, R_{e0}, or the transfer resistance R_{ep} between two electrode elements which are on the same side of the surface and are p indices apart, l_1 is replaced by l_e and M by $2M_e$ in equations (5) and (6). For the transfer $R_{n,m}(\neq R_{m,n})$ between a line source m and a line source center point n where one is an electrode element and the other is a stem element, or between two electrode elements on opposite sides of the surface of the earth, no simple indexed equation is possible and (2) must be used directly. For a nonzero V_s, the result is shown at the bottom of the page in (7). Since the stem and electrode are taken to be perfectly conducting in this initial formulation, the entire stem settles at a voltage V_d, and the electrode settles at V_d–V_s. The above transfer matrix has been compacted using the fact that $I_n = I_{-n}$ and $V_n = V_{-n}$, making the nth row of the uncompacted matrix a copy of the $10-n$th row. Compacting is simplified because $R_{m,n} = R_{-m,-n}$. Furthermore, it is useful to retain $I_0/2$ rather than I_0 as a variable.

Non-zero source, surface, longitudinal, and joint resistance can now be introduced. A surface resistance $R_{\rm dc}$, expressed in Ωm^2, can be taken into account by an addition to the self-transfer resistances for the elemental line sources as follows [7]:

$$R_0' = R_0 + \frac{R_{\rm dc} M}{4\pi l_1 a}$$
$$R_{e0}' = R_{e0} + \frac{R_{\rm dc} M_e}{2\pi l_e a} \tag{8}$$

where R_0' and R_{e0}' are the modified self-transfer resistances.

The longitudinal and joint resistances of the cylinder and the internal resistance of the voltage source V_s can be taken into account as shown in Fig. 5. Referring to Fig. 5, it is easy to see that

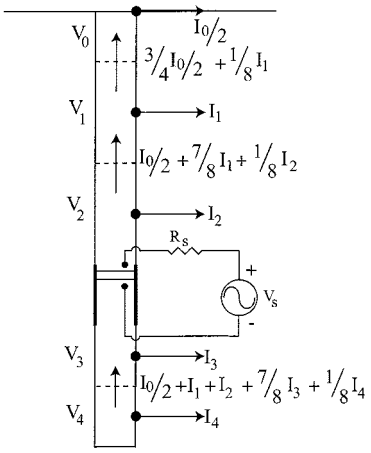

Fig. 5. Sectioned stem and electrode showing current flow into the earth and longitudinal current flow.

the longitudinal currents between sections are simply related to the individual line current sources I_n. Each longitudinal current labeled in Fig. 5 is the average current flowing between the centers of adjacent elements assuming a linearly decreasing flow in each element. The potential of the midpoint of the section straddling the surface of the earth is taken to be V_d and hence

$$\begin{aligned}
V_0 &= V_d \\
V_1 &= V_0 + \left(R_{ld} + \frac{R_j}{L_j}\frac{2l_1}{M}\right)\left(\frac{3}{4}\frac{I_0}{2} + \frac{I_1}{8}\right) \\
V_2 &= V_1 + \left(R_{ld} + \frac{R_j}{L_j}\frac{2l_1}{M}\right)\left(\frac{I_0}{2} + \frac{7}{8}I_1 + \frac{I_2}{8}\right) \\
V_3 &= V_2 + \frac{R_{ld}}{2}\left(\frac{I_0}{2} + I_1 + \frac{3}{4}I_2\right) \\
&\quad + \frac{R_{le}}{2}\left(\frac{I_0}{2} + I_1 + I_2 + \frac{I_3}{4}\right) + R_s'\left(\frac{I_0}{2} + I_1 + I_2\right) \\
V_4 &= V_3 + \left(R_{le} + \frac{R_j}{L_j}\frac{l_e}{M_e}\right)\left(\frac{I_0}{2} + I_1 + I_2 + \frac{7}{8}I_3 + \frac{I_4}{8}\right).
\end{aligned} \tag{9}$$

The resistances R_{ld} and R_{le} are the longitudinal resistances of a stem section and electrode section, respectively, and are given by

$$R_{ld} = \frac{2l_1\rho_m}{M\pi(a^2-b^2)}$$
$$R_{le} = \frac{l_e\rho_m}{M_e\pi(a^2-b^2)} \tag{10}$$

$$\begin{bmatrix} V_d \\ V_d \\ V_d \\ V_d - V_s \\ V_d - V_s \end{bmatrix} = \begin{bmatrix} 2R_0 & 2R_1 & 2R_2 & 2R_{0,3} & 2R_{0,4} \\ 2R_1 & R_0+R_2 & R_1+R_3 & R_{1,3}+R_{1,-3} & R_{1,4}+R_{1,-4} \\ 2R_2 & R_1+R_3 & R_0+R_4 & R_{2,3}+R_{2,-3} & R_{2,4}+R_{2,-4} \\ 2R_{3,0} & R_{3,1}+R_{3,-1} & R_{3,2}+R_{3,-2} & R_{e0}+R_{3,-3} & R_{e1}+R_{3,-4} \\ 2R_{4,0} & R_{4,1}+R_{4,-1} & R_{4,2}+R_{4,-2} & R_{e1}+R_{4,-3} & R_{e0}+R_{4,-4} \end{bmatrix} \begin{bmatrix} I_0/2 \\ I_1 \\ I_2 \\ I_3 \\ I_4 \end{bmatrix} \tag{7}$$

where

ρ_m = resistivity of the tubular stock
a = outer radius of the tubular stock
b = inner radius of the tubular stock.

The resistance R'_s is the combined resistance of the voltage source internal resistance and the gap resistance, given by

$$R'_s = R_s + \frac{R_{le} M_e l_{gap}}{l_e}. \tag{11}$$

The resistance R_j is the joint resistance per joint, and the length L_j is the distance between joints. The joint resistance is treated as if it were uniformly distributed over the stem and electrode lengths. Substitution for V_0, V_1, V_2, V_3, V_4 into (7) yields

$$\begin{bmatrix} V_d \\ V_d \\ V_d \\ V_d - V_s \\ V_d - V_s \end{bmatrix} = [R] \begin{bmatrix} I_0/2 \\ I_1 \\ I_2 \\ I_3 \\ I_4 \end{bmatrix} \tag{12}$$

with $[R]$, as shown at the bottom of the page in (13), where

$$R'_{ld} = R_{ld} + \frac{R_j}{L_j}\frac{2l_1}{M}$$
$$R'_{le} = R_{le} + \frac{R_j}{L_j}\frac{l_e}{M_e}$$
$$R_a = \frac{R_{le}}{2} + \frac{R_{ld}}{2}$$
$$R'_a = R'_l e + R'_s$$

and $R''_{i,j}$ is the element in the ith row and jth column in matrix (7). Equation (13) can be inverted to yield

$$\begin{bmatrix} I_0/2 \\ I_1 \\ I_2 \\ I_3 \\ I_4 \end{bmatrix} = [R^{-1}] \begin{bmatrix} V_d \\ V_d \\ V_d \\ V_d \\ V_d \end{bmatrix} + [R^{-1}] \begin{bmatrix} 0 \\ 0 \\ 0 \\ -V_s \\ -V_s \end{bmatrix}. \tag{14}$$

The restriction that the currents $I_0/2$, I_1, I_2, I_3, I_4 must sum to zero allows a determination of V_d using

$$V_d = \frac{V_s \sum_{m=1}^{N} \sum_{n=N-M_e}^{N} R^{-1}_{m,n}}{\sum_{m=1}^{N} \sum_{n=1}^{N} R^{-1}_{m,n}} \tag{15}$$

where $R^{-1}_{m,n}$ is the element in the mth row and nth column of the inverted resistance matrix having N rows and N columns. The potential Φ on the surface of the Earth at a distance r_1 from the top of the stem can now be calculated using (3) to give

$$\begin{aligned} \Phi = {} & \frac{\frac{I_0}{2}\rho M}{4\pi l_1} \ln\left[\frac{l_1 + \sqrt{l_1^2 + M^2 r_1^2}}{M r_1}\right] \\ & + \sum_{n=1}^{(M-1)/2} \frac{I_n \rho M}{8\pi l_1} \\ & \cdot \ln\left[\frac{2n+1+\sqrt{(2n+1)^2 + \left(\frac{M r_1}{l_1}\right)^2}}{2n-1+\sqrt{(2n-1)^2 + \left(\frac{M r_1}{l_1}\right)^2}}\right] \\ & + \sum_{n=((M-1)/2)+1}^{((M-1)/2)+M_e} \frac{I_n \rho M_e}{4\pi l_e} \\ & \cdot \ln\left[\frac{2n+1+\sqrt{(2n+1)^2 + \left(\frac{2M_e r_1}{l_e}\right)^2}}{2n-1+\sqrt{(2n-1)^2 + \left(\frac{2M_e r_1}{l_e}\right)^2}}\right]. \end{aligned} \tag{16}$$

This can be used to yield the $V_d - \Phi_{r1}$ to V_s ratio, which is a measure of the channel attenuation. The driving point resistance is given by the ratio of V_s to the sum of the electrode section currents.

V. AC Effects

The frequency dependence of the internal and external impedance of tubular stock, the impedance of the stock-earth

$$[R] = \begin{bmatrix} R''_{0,0} & R''_{0,1} & R''_{0,2} & R''_{0,3} & R''_{0,4} \\ R''_{1,0} - \frac{3}{4}R'_{ld} & R''_{1,1} - \frac{1}{8}R'_{ld} & R''_{1,2} & R_{1,3} + R''_{1,3} & R''_{1,4} \\ R''_{2,0} - \frac{7}{4}R'_{ld} & R''_{2,1} - R'_{ld} & R''_{2,2} - \frac{1}{8}R'_{ld} & R''_{2,3} & R''_{2,4} \\ R''_{3,0} - \frac{7}{4}R'_{ld} - R_a - R'_s & R''_{3,1} - R'_{ld} - R_a - R'_s & R''_{3,2} - \frac{1}{8}R'_{ld} - \frac{3}{8}R_{ld} - \frac{R_{le}}{2} - R'_s & R''_{3,3} - \frac{R_{le}}{8} & R''_{3,4} \\ R''_{4,0} - \frac{7}{4}R'_{ld} - R_a - R'_a & R''_{4,1} - R'_{ld} - R_a - R'_a & R''_{4,2} - \frac{1}{8}R'_{ld} - \frac{3}{8}R_{ld} - \frac{R_l e}{2} - R'_a & R''_{4,3} - \frac{7}{8}R'_{le} - \frac{R_{le}}{8} & R''_{4,4} - \frac{1}{8}R'_{le} \end{bmatrix}. \tag{13}$$

interface, and the propagation of electric fields through the Earth are now considered.

A. Internal Impedance

The internal impedance of tubular stock Z_{iac} can be calculated as outlined below

$$Z_{i\mathrm{ac}} = R_{i\mathrm{dc}}\left[\frac{R_{i\mathrm{ac}}}{R_{i\mathrm{dc}}}\right] + j\omega L_{i\mathrm{dc}}\left[\frac{L_{i\mathrm{ac}}}{L_{i\mathrm{dc}}}\right] \tag{17}$$

where

$$R_{i\mathrm{dc}} = \frac{l_1\rho_m}{\pi(a^2-b^2)} \tag{18}$$

$$L_{i\mathrm{dc}} = \frac{\mu l_1}{8\pi}\left[\frac{a^2-3b^2}{a^2-b^2} + \frac{4b^4\ln\left[\frac{a}{b}\right]}{(a^2-b^2)^2}\right] \tag{19}$$

a = outer radius of the tubular stock;
b = inner radius of the tubular stock;
l_1 = length of the stock;
$\mu = \mu_r\mu_0$ where μ_r is the relative permeability and μ_0 is the free space permeability.
of the stock material and μ_0 is the

$$\frac{R_{i\mathrm{ac}}}{R_{i\mathrm{dc}}} = \frac{1}{2} + \left[\frac{mt}{\sqrt{2}} - \frac{1}{2}\right]\left[1 - \frac{7}{8}\left[\frac{t}{d}\right] - \frac{1}{4}\left[\frac{t}{d}\right]^2\right] \quad \text{for } \frac{R_{i\mathrm{ac}}}{R_{i\mathrm{dc}}} \geq 1.0 \tag{20}$$

$$\frac{L_{i\mathrm{dc}}}{L_{i\mathrm{ac}}} = \frac{2mt}{3\sqrt{2}}\left[1 - 2\left[\frac{t}{d}\right]^3\right] \text{ for } \frac{L_{i\mathrm{dc}}}{L_{i\mathrm{ac}}} \geq 1.0 \tag{21}$$

$t = a - b$
$d = 2a$
$m^2 = \dfrac{\omega\mu}{\rho_m}$

and ρ_m is the resistivity of the stock material [8]. In these empirically determined equations, $R_{i\mathrm{ac}}/R_{i\mathrm{dc}}$ and $L_{i\mathrm{dc}}/L_{i\mathrm{ac}}$ should be set to 1.0 if (20) and (21) yield a result less than unity.

To account for the high frequency internal impedance of the tubular members, R_{ld} in (13) should be replaced by $Z_{i\mathrm{ac}}$, and R_{le} in (13) should be replaced by $Z_{i\mathrm{ac}}$ calculated with l_1 in (18) and (19) replaced by l_e.

B. External Inductance

The external inductance of an isolated cylinder of length l and outer radius a is given by [9]

$$L_{external} = \frac{\mu_0 l}{2\pi}\left(\ln\frac{2l}{a} - 1\right). \tag{22}$$

This term is multiplied by $j\omega$ and added to R_{ld} and R_{le} in (10), with the cylinder length l equal to $2l_1/M$ and l_e/M_e, respectively. However, the external inductance of a stem of length $2l_1$ is not equal to the sum of the inductances of M sections each of length $2l_1/M$ and it is therefore necessary to include mutual inductances between sections as outlined in reference [10].

The transfer impedance (i.e., $j\omega$ times the mutual inductance but with earth propagation effects not considered) between a section of length l_s and a section of length l'_s with the centers of the sections distances e and f below ground, respectively, is given by $X(h=f) - X(h=f-l'_s)$ (see Appendix) with X given by

$$X = \frac{j\omega\mu_0}{4\pi}\left(\nu\sinh^{-1}\frac{\nu}{a} - \sqrt{\nu^2+a^2} - (\nu-l_s)\sinh^{-1}\frac{\nu-l_s}{a} + \sqrt{(\nu-l_s)^2+a^2}\right) \tag{23}$$

where $\nu = e - h$. The voltages V_n of Fig. 5 become V'_n

$$\begin{aligned}
V'_0 &= V_d \\
V'_1 &= V_1 + X_{1,2}\left(\frac{I_0}{2} + I_1 + \frac{I_2}{2}\right) + (X_{1,gap} + X_{1,3})\left(\frac{I_0}{2} + I_1 + I_2\right) + X_{1,3}\frac{I_3}{2} + X_{1,4}\left(\frac{I_0}{2} + I_1 + I_2 + I_3 + \frac{I_4}{2}\right) \\
V'_2 &= V'_1 - V_1 + V_2 + X_{2,1}\left(\frac{I_0}{2} + \frac{I_1}{2}\right) + (X_{2,gap} + X_{2,3})\left(\frac{I_0}{2} + I_1 + I_2\right) + X_{2,3}\frac{I_3}{2} + X_{2,4}\left(\frac{I_0}{2} + I_1 + I_2 + I_3 + \frac{I_4}{2}\right) \\
V'_3 &= V'_2 - V_2 + V_3 + X_{3,1}\left(\frac{I_0}{2} + \frac{I_1}{2}\right) + X_{3,2}\left(\frac{I_0}{2} + I_1 + \frac{I_2}{2}\right) + X_{3,gap}\left(\frac{I_0}{2} + I_1 + I_2\right) + X_{3,4}\left(\frac{I_0}{2} + I_1 + I_2 + I_3 + \frac{I_4}{2}\right) \\
V'_4 &= V'_3 - V_3 + V_4 + X_{4,1}\left(\frac{I_0}{2} + \frac{I_1}{2}\right) + X_{4,2}\left(\frac{I_0}{2} + I_1 + \frac{I_2}{2}\right) + (X_{4,gap} + X_{4,3}) \cdot \left(\frac{I_0}{2} + I_1 + I_2\right) + X_{4,3}\frac{I_3}{2}
\end{aligned} \tag{24}$$

where the V_n are the V_n of (9). The longitudinal currents used to calculate the inductive interactions are the average values of the currents between the ends of the sections.

The voltage induced in a below-ground element by an above-ground current is opposite in sign to the voltage induced in that element by a below-ground current (see Appendix). Thus, each mutual coupling term in (24) has a positive and a negative component

$$X_{n,m} = X'_{n,m} - X'_{n,-m} \tag{25}$$

where X' is calculated directly from (23).

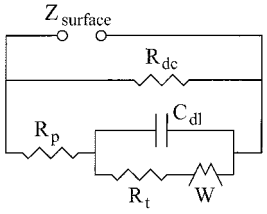

Fig. 6. Equivalent circuit model for the interface impedance between the well casing and the earth.

C. Interface Impedance

An interface impedance is used to model the current transfer mechanism between the metal casing and the adjacent earth. The equivalent circuit model for this impedance $Z_{surface}$ used by Wait and Williams [11], is shown in Fig. 6. Typical values for steel with a zinc phosphate coating given by Wait and Williams are

$$R_p = 1\ \Omega\mathrm{m}^2$$
$$R_t = 0.1\ \Omega\mathrm{m}^2$$
$$R_{\mathrm{dc}} = 10\ \Omega\mathrm{m}^2$$

and

$$C_{dl} = 75\ \mu\mathrm{F/m}^2.$$

The Warburg impedance W is given by

$$W = \nu/(2j\omega)^{1/2}\ \Omega\mathrm{m}^2 \tag{26}$$

where a typical value of ν is

$$\nu = 10\ \Omega\mathrm{m}^2 s^{-1/2}.$$

$Z_{surface}$ replaces R_{dc} in (8) and has a low frequency limit equal to R_{dc}.

D. Propagation Effects

The method used to incorporate propagation effects in the earth is based on a modification of an analysis of a vertical subsurface line current source and a potential pick up array located on the surface of the earth first used in [10] and described more fully in the Appendix. In this procedure, each transfer resistance R in (13), except for the self-transfer resistances, and each transfer impedance X in (24) should be replaced by

$$Z = Re^{-\gamma r_p} \quad \text{or} \quad Z = Xe^{-\gamma r_p} \tag{27}$$

where r_p is the distance between the center of the line source in question and the center of the stem or electrode outer surface of the affected element, and $\gamma^2 = j\omega\mu_0\sigma$ (see Appendix). Between stem (not electrode) elements, for instance

$$r_p^2 = a^2 + \left[\frac{2pl_1}{M}\right]^2, \quad p = 1 \text{ to } (M-1).$$

Similarly

$$e^{-\gamma r_n}$$

must multiply each term of (16), where r_n is the distance to the pickup point on the surface of the earth from the center of the line source in question. For stem elements, r_n is given by

$$r_n^2 = r_1^2 + \left[\frac{2nl_1}{M}\right]^2, \quad n = 0 \text{ to } \left[\frac{M-1}{2}\right]$$

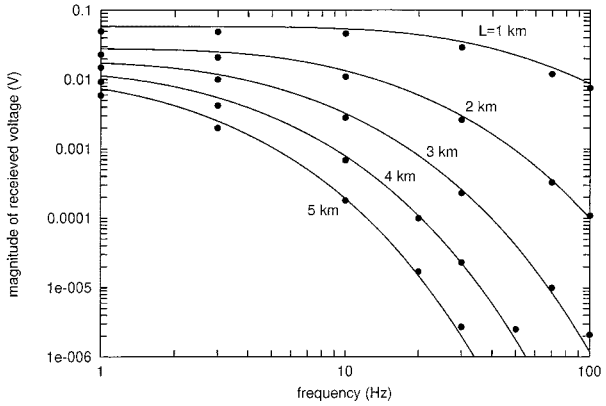

Fig. 7. Comparison of received voltage versus frequency using the methods of this paper (lines) against Xia's and Chen's results (points) for an earth resistivity of 20 Ωm and a source providing a constant power of 10 W.

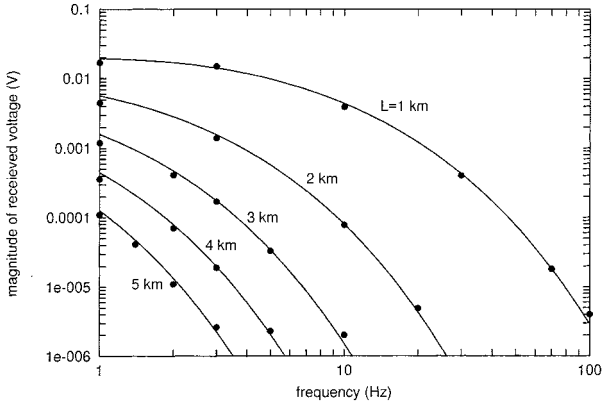

Fig. 8. Comparison of received voltage versus frequency using the methods of this paper (lines) against Xia's and Chen's results (points) for an earth resistivity of 2.5 Ωm and a source providing a constant power of 10 W.

with r_1 being the horizontal distance from the pickup point to the top of the stem.

VI. Modeling Results

A fast personal computer program with a convenient input screen has been developed to carry out simulation calculations. As a first check, the examples given by Xia and Chen [12] for a perfectly conducting stem and electrode were simulated. The results of these simulations are compared to Xia and Chen's work in Figs. 7 and 8. Xia and Chen used the following parameters in their examples:

$$2a = 0.16\ \mathrm{m}$$
$$l_{gap} = 10\ \mathrm{m}$$
$$l_e = 10\ \mathrm{m}$$

and

$$L = l_{gap} + l_e + l_1.$$

The receiving antenna had one end connected to the stem and the other end connected to the earth 50 m away from the stem. The amplitude of the voltage source was chosen to deliver 10 W of power to the stem-electrode system at all frequencies. Although

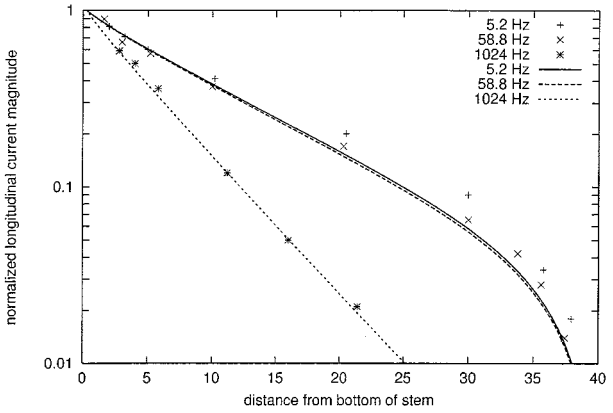

Fig. 9. Normalized longitudinal current as a function of distance above the bottom of the stem. The points were measured experimentally, the lines calculated. The experimental situation was a 40 m, 2.54 cm diameter steel pipe with a wall thickness of 2.2 mm, a relative magnetic permeability of 27, and a longitudinal resistivity of 2.38×10^{-7} Ωm, a 1 m electrode and an unspecified gap length, submerged into the Mediterranean, which had a measured resistivity of between 4 and 5 Siemens per meter. The situation was modeled with the same parameters, taking the sea resistivity to be 0.2 Ωm, the gap length to be 2 m, and no surface impedance.

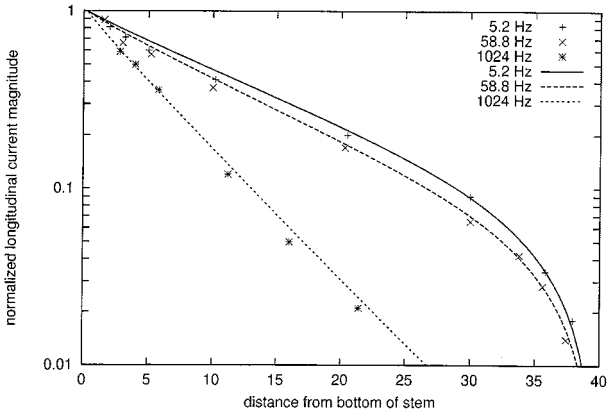

Fig. 10. The situation of Fig. 9 with surface impedance (both stem and electrode) parameters of $R_{\rm dc} = 0.04$ Ωm^2, $R_t = 0.001$ Ωm^2, $\nu = 0.085$ Ωm^{2}s$^{-0.5}$, $C_{dl} = 7.5 \times 10^{-5}$ Fm^{-2}. All other surface impedance parameters were taken to be zero.

the assumption of zero stem and electrode resistivity is not realistic, the good agreement between the two sets of results provides an important confirmation of the technique used in this work.

DeGauque and Grudzinski [13] have taken normalized measurements of longitudinal current along an uncoated steel stem immersed in sea water. When the resistivity of the material in which the stem is embedded is as low as that of sea water, longitudinal stem impedance and stem surface impedances are important. Results using the model presented here with zero surface impedance are compared with DeGauque and Grudzinski's experimental results in Fig. 9. A small surface impedance was added to fine tune a fit to the experimental results as shown in Fig. 10. The excellent agreement between measurements and simulation results in Figs. 9 and 10 provides a further confirmation of the techniques used here, and particularly, the manner in which longitudinal and surface impedance are handled.

The importance of metal resistivity is highlighted in Figs. 11 and 12, in which Xia and Chen's situations of Figs. 7 and 8 have been modified by taking the metal resistivity to be 2×10^{-7} Ωm [14] and by adding a small joint resistance. These figures show that metal resistivity and conductor joint resistance must be considered for accurate modeling.

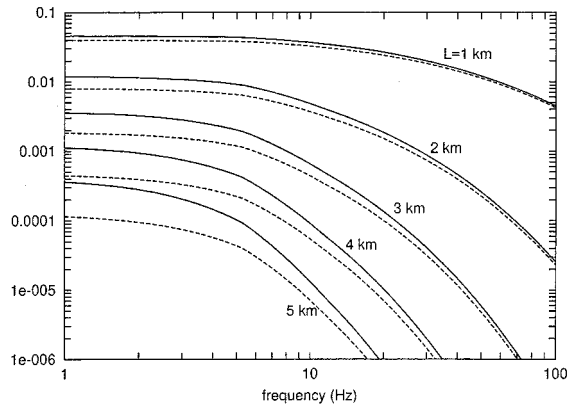

Fig. 11. Results for Xia and Chen's example with a metal resistivity of 2×10^{-7} Ωm, a relative metal permeability of 100, and a wall thickness of 1 cm, and joint resistance varying from zero (solid lines) to 0.25 mΩ (dashed lines) per 10 m of conductor length. The earth resistivity is 20 Ωm.

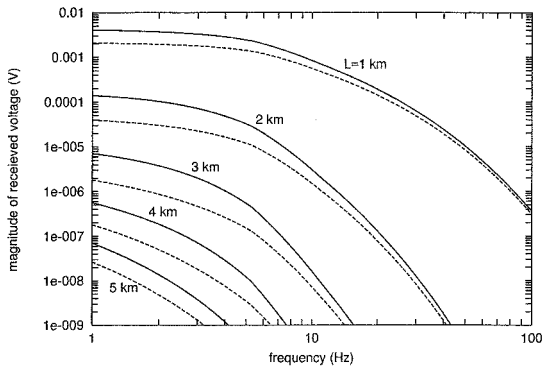

Fig. 12. Results for Xia and Chen's example with a metal resistivity of 2×10^{-7} Ωm, a relative metal permeability of 100, and a wall thickness of 1 cm and joint resistance varying from zero (solid lines) to 0.25 mΩ (dashed lines) per 10 m of conductor length. The earth resistivity is 2.5 Ωm.

A plot of received voltage as a function of stem length, earth resistivity and joint resistance is given in Fig. 13 and a plot of driving point impedance magnitude and phase as a function of electrode length and earth resistivity for two stem lengths is given in Fig. 14. From Fig. 14, it can be seen that the driving point impedance is essentially resistive and practically independent of stem length for this range of stem and electrode lengths. The driving point resistances can consequently be calculated to within 10% in the parameter range above the 10% line indicated in Fig. 14 using

$$R_{DP} = \frac{\rho}{2\pi l_e} \ln\left(\frac{l_e}{a}\right) + R_s \tag{28}$$

with R_s, the voltage source resistance, set to zero. The implication is that the received voltage magnitude depends directly on the magnitude of the electrode current, which is determined almost entirely by V_s and R_{DP}. Equation (28) can therefore be used to scale the results given in Fig. 13 appropriate for $V_s =$ 1 V, $l_e =$10 m, $R_s = 0$ Ω and joint resistance equal to zero to obtain the received voltage magnitude for other values of V_s, l_e and R_s. For example, if $V_s = 5$ V, $l_e = 20$ m, $R_s = 1$ Ω, and

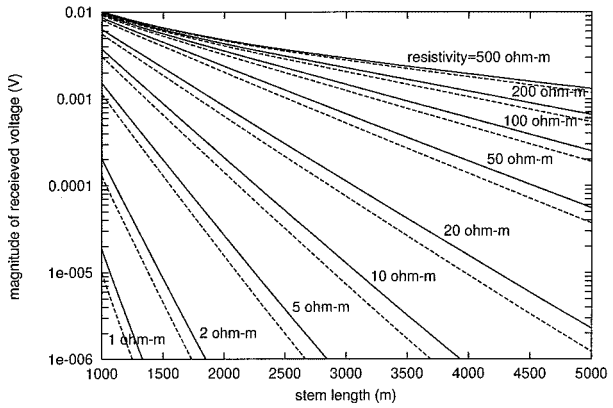

Fig. 13. Received voltage magnitude results for Xia and Chen's example as a function of stem length and earth resistivity, with a metal resistivity of 2×10^{-7} Ωm, a relative metal permeability of 100, a wall thickness of 1 cm, a 1 volt source with no source resistance R_s, no surface impedance, a frequency of 10 Hz, and a joint resistance varying from zero (solid lines) to 0.25 mΩ (dashed lines) per 10 m of conductor length.

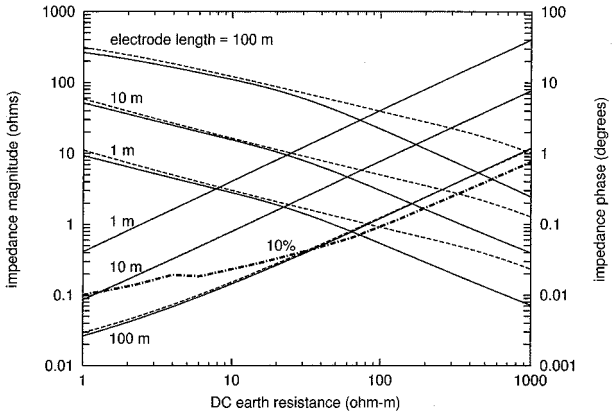

Fig. 14. Driving point impedance results for Xia and Chen's example as a function of earth resistivity and electrode length, with a metal resistivity of 2×10^{-7} Ωm, a relative metal permeability of 100, a wall thickness of 1 cm, zero joint resistance, a frequency of 10 Hz, a 1 V source with no source resistance, zero surface impedance, and stem length varying from 1000 m (solid lines) to 5000 m (dashed lines). The phase decreases with earth resistivity. All magnitude values above the dashed 10% line can be calculated to within 10% by (28) for $R_s = 0$.

$\rho = 20$ Ωm, then $R_{DP} = 1.9$ Ω. Since R_{DP} is 1.5 Ω for $l_e =$ 10 m, $\rho = 20$ Ωm and $R_s = 0$ Ω, the received voltage of 1.1 $\times 10^{-4}$ V for $\rho = 20$ Ωm, $l_1 = 3000$ m, joint resistance equal to zero with $V_s = 1$ V given in Fig. 13 would be multiplied by (5/1)(1.5/1.9) to give a received voltage of 4.5×10^{-4}, in good agreement with a value of 4.7×10^{-4} V obtained using the simulation program.

VII. Conclusions

A line current technique for modeling a downhole to surface communication channel consisting of a long vertical cylinder (the stem) and an isolated downhole in line cylinder (the electrode) embedded in a homogeneous earth has been developed. Simulation results are in good agreement with Xia and Chen's work [12] dealing with the zero metal resistivity case and with DeGauque and Grudzinski's experimental work [13] dealing with an uncoated steel pipe submerged in sea water. The model

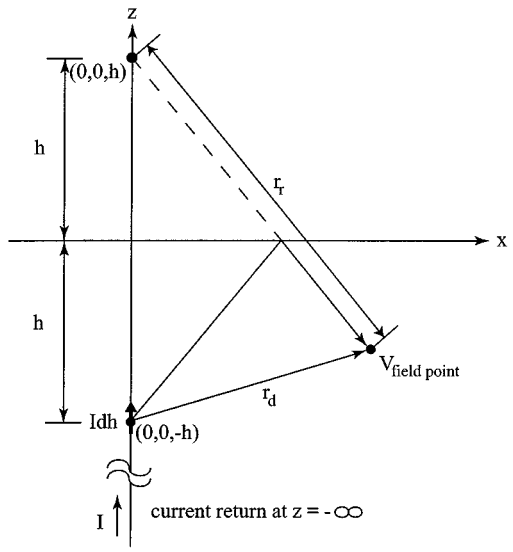

Fig. 15. Coordinate system for evaluating the effects of a current dipole Idh at a subsurface point $z = -h$.

described in this work takes into account cylinder longitudinal and surface impedance, cylinder joint resistance, voltage source resistance and earth propagation effects. Extensive modeling work can now be carried out in tens of seconds to ascertain whether or not data transmission is possible in a particular field situation or to assist in the design of downhole to surface communication systems.

Appendix

The quasistatic magnetic vector potential $\vec{A}$ for $z < 0$ for a dipole Idh at $z = -h$, as shown in Fig. 15 can be written as [15] $\vec{A} = \vec{k}A_z$ where

$$\vec{A_z} = \frac{\rho I dh}{4\pi}\left[\frac{e^{-\gamma r_d}}{r_d} - \frac{e^{-\gamma r_r}}{r_r}\right] \tag{A1}$$

and hence, the electric field can be expressed as

$$\vec{E} = -\gamma^2 \vec{A} - \bigtriangledown V \tag{A2}$$

where the scalar potential V is given by $V = -\rho \bigtriangledown \bullet \vec{A}$. It is then easy to show that V due to a current flowing from $z = -\infty$ and out at $z = -h$ is given by

$$V = \frac{\rho}{4\pi}\left[\frac{e^{-\gamma r_d}}{r_d} + \frac{e^{-\gamma r_r}}{r_r}\right] \tag{A3}$$

where r_d and r_r can be interpreted as the direct and reflected distances as shown in Fig. 15. This expression justifies the use of the exponential factor in the transfer resistances as outlined in Section V.D of this paper since each of the currents I_n can be considered to originate at $z = -\infty$. The currents I_n sum to zero and consequently cancel completely below the bottom end of the electrode [7], [11].

The nonconservative portion of the field $\vec{E} = -\gamma^2 \vec{A}$ reduces to $E_z = -\gamma^2 A_z$ and can be taken into account by an external self-inductance of each section of the stem, gap and electrode and by attenuated mutual inductances between these sections.

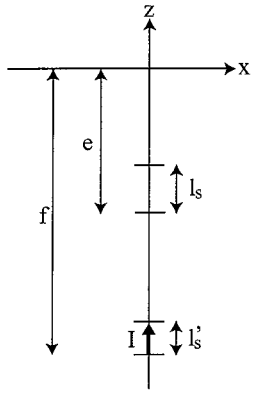

Fig. 16. Length of pipe whose bottom is at depth f carries current I and induces a voltage in a length of pipe whose bottom is at depth e.

The potential of the bottom with respect to the top of a section of cylinder due to a subsurface dipole is given by

$$\int_{e-l_s}^{e} E_z\,dz = \frac{-j\omega\mu_0 I\,dh}{4\pi}\int_{e-l_s}^{e}\frac{dz}{\sqrt{a^2+(z-h)^2}}. \quad \text{(A4)}$$

The cylinder has a length l_s, and its bottom is at a depth e. The dipole is at a depth h. The situation is shown in Fig. 16. The expression for E_z is the first term of (A1) multiplied by $-\gamma^2$ with the exponential factor taken to be unity, i.e., earth propagation effects are ignored at this stage. Integration yields

$$\int_{e-l_s}^{e} E_z\,dz = \frac{j\omega\mu_0 I\,dh}{4\pi} \cdot\left[\sinh^{-1}\left(\frac{e-h}{a}\right)-\sinh^{-1}\left(\frac{e-l_s-h}{a}\right)\right]. \quad \text{(A5)}$$

A second integration in dh from $f-l_s'$ to f where l_s' is the length of the current-carrying section and f is the depth of the bottom of that section yields the following expression for the voltage of the bottom with respect to the top of the section of length l_s:

$$I[X(h=f)-X(h=f-l_s')] \quad \text{(A6)}$$

where

$$X=\frac{j\omega\mu_0}{4\pi}\left(\nu\sinh^{-1}\frac{\nu}{a}-\sqrt{\nu^2+a^2} -(\nu-l_s)\sinh^{-1}\frac{\nu-l_s}{a} +\sqrt{(\nu-l_s)^2+a^2}\right) \quad \text{(A7)}$$

and $\nu=e-f$. Note that e and f refer to the depths of the bottoms of the current-carrying and affected lengths respectively. These points are at the centers of the sections as defined in this paper since the length of pipe that carries a constant longitudinal current is that between section centers.

The impedance due to the external self-inductance of the section l_s is obtained by setting $e=f$ and $l_s'=l_s$ provided the radius is small compared to the section length and $|\gamma l_s|\ll 1$ so that the exponential factor can be taken to be unity. This produces (23).

When (A7) is applied between two sections of length l_s and l_s' such that $|\gamma l_s|,|\gamma l_s'|\ll 1$, the exponential factor can now be introduced by multiplying (A7) by $e^{-\gamma r_p}$ where r_p is the distance between the centers of l_s and l_s'.

The second term of A_z, $-e^{-\gamma r_r}/r_r$, deals with imaged current-carrying elements and leads to an equation identical to (A7) with the appropriate adjustments of distances and sign and is included in the transfer matrix through the second term of (25).

REFERENCES

[1] D. A. Hill and J. R. Wait, "Electromagnetic basis of drill-rod telemetry," *Electron. Lett.*, vol. 14, pp. 532–533, Aug. 1978.
[2] J. R. Wait and D. A. Hill, "Theory of transmission of electromagnetic waves along a drill rod in conducting rock," *IEEE Trans. Geosci. Electron.*, vol. GE-17, pp. 21–24, Apr. 1979.
[3] J. Bhagwan and F. N. Trofimenkoff, "Electric drill stem telemetry," *IEEE Trans. Geosci. Remote Sensing*, vol. GE-20, pp. 193–197, Apr. 1982.
[4] ——, "Drill stem resistance effects in electric telemetry links," *IEEE Trans. Geosci. Remote Sensing*, vol. GE-21, pp. 141–144, Apr. 1983.
[5] D. Silverman and R. Fearon, "Well Signaling System," U.S. Patent 2 354 887, Aug. 1, 1944.
[6] R. H. Johnston, F. N. Trofimenkoff, and J. W. Haslett, "Resistivity response of a homogeneous earth with a finite length contained vertical conductor," *IEEE Trans. Geosci. Remote Sensing*, vol. GE-25, pp. 414–421, July 1987.
[7] J. R. Wait, "Resistivity response of a homogeneous earth with a contained vertical conductor," *IEEE Trans. Geosci. Remote Sensing*, vol. GE-21, pp. 109–113, Jan. 1983.
[8] F. N. Trofimenkoff, R. H. Johnston, J. W. Haslett, and B. Hriskevich, "Impedance of tubular stock at high frequencies," *Can. J. Elect. Comp. Eng.*, vol. 14, no. 4, pp. 135–137, 1989.
[9] *Electronics Designers Handbook*, McGraw-Hill, New York, 1977.
[10] R. H. Johnston, F. N. Trofimenkoff, and J. W. Haslett, "The complex resistivity response of a homogeneous earth with a finite-length contained vertical conductor," *IEEE Trans. Geosci. Remote Sensing*, vol. 30, pp. 46–54, Jan. 1992.
[11] J. R. Wait and J. T. Williams, "EM and IP response of a steel well casing for a four-electrode surface array—Part I: Theory—Part II: Numerical results," *Geophys. Prospecting*, vol. 33, pp. 723–745, Aug. 1985.
[12] M. Y. Xia and Z. Y. Chen, "Attenuation predictions at extremely low frequencies for measurement-while-drilling electromagnetic telemetry system," *IEEE Trans. Geosci. Remote Sensing*, vol. 31, pp. 1222–1228, Nov. 1993.
[13] P. DeGauque and R. Grudzinski, "Propagation of electromagnetic waves along a drillstring of finite conductivity," *SPE Drilling Eng.*, pp. 127–134, June 1987.
[14] F. N. Trofimenkoff, J. W. Haslett, and R. H. Johnston, "Measurement of resistivity and permeability of tubular stock," *Can. J. Elect. Comput. Eng.*, vol. 18, no. 1, pp. 41–43, 1993.
[15] J. R. Wait, *Geo-Electromagnetism*. New York: Academic, 1982, p. 179.

F. N. Trofimenkoff (M'63–SM'69) was born in Veregin, SK, Canada, on August 10, 1934. He received the B.E. degree in engineering physics and the M.Sc. degree in physics, both from the University of Saskatchewan, saskatoon, SK, Canada, in 1957 and 1959, respectively. He received the Ph.D. degree in electrical engineering from the Imperial College of Science and Technology, London, U.K., in 1962.

From 1957 to 1959, he worked on instrumentation for accurate humidity measurement in the Division of Building Research, National Research Council of Canada, and from 1962 to 1966, he was an Assistant Professor of electrical engineering, University of Saskatchewan. In 1966, he moved to the Electrical Engineering Department, University of Calgary, Calgary, BC, Canada, where he is currently a Professor Emeritus and a Faculty Professor. His interests are in the circuits and device area and instrumentation related to the petroleum industry.

Michael Segal was born in Leningrad, Russia, on July 11, 1976. He received the B.Sc. degree from the University of Alberta, Edmonton, AB, Canada, in 1997.

He is currently a Research Engineer in the Electrical and Computer Engineering Department, University of Calgary, Calgary, BC, Canada.

Dr. Segal received the gold medal in engineering physics from the Association of Professional Engineers, Geologists, and Geophysicists of Alberta in 1997

Allan Klassen received the B.Sc. and M.Sc. degrees in electrical engineering from the University of Calgary, Calgary, BC, Canada, in 1981 and 1984, respectively.

He currently develops digital signal processing algorithms and systems involving three–dimensional (3-D) audio, reverberation, sample rate conversion, and music synthesis for audio applications such as hearing aids and sound cards. His clients include QSound Labs, Inc., Calgary, BC, Canada, and Starkey Labs, Inc., Minneapolis, MN.

J. W. Haslett (S'64–M'66–SM'79) was born in North Battleford, SK, Canada, on September 27, 1944. He received the B.Sc. degree in electrical engineering from the University of Saskatchewan, Saskatoon, SK, Canada, in 1966, and the M.Sc. and Ph.D. degrees from the University of Calgary, Calgary, AB, Canada, in 1968 and 1970, respectively.

He subsequently joined the Department of Electrical Engineering, University of Calgary, where he is currently a Professor. From 1970 to 1975, his main research interest was in the area of noise mechanisms in solid-state devices. Since 1975, his interests have shifted to low light CCD imagers for spacecraft applications, high frequency R-C active filter networks, and specialized instrumentation systems related to drill-stem testing of oil and gas wells.